X-ray strain analysis at high pressure: Effect of plastic deformation in MgO

Li Li,[a] Donald J. Weidner, Jiuhua Chen, Michael T. Vaughan, and Maria Davis
Department of Geosciences and Mineral Physics Institute, Stony Brook University, Stony Brook, New York 11794-2100

William B. Durham
University of California, Lawrence Livermore National Laboratory, P.O. Box 808, Livermore, California 94550

(Received 8 October 2003; accepted 18 March 2004)

The factors that control the stress–strain state of a polycrystal under differential stress depend on whether or not plastic deformation has occurred in the solid. If not, then the elastic properties with the constraints of the Reuss–Voigt bounds limit this relationship. If plastic deformation becomes important then the Taylor and Sachs models are relevant. These models assume that the plastic process is enabled by dislocation flow on specific lattice planes and specific Burger's vectors. Then, the relationship between stress and strain is controlled by the orientation of an individual grain with respect to the stress field, von Mises criterion, and the critical resolved stress on the dislocation that is necessary for flow. We use a self-consistent model to predict the flow stress during the plastic deformation of polycrystalline MgO with a slip system of $\{110\}\langle 1\bar{1}0\rangle$, $\{111\}\langle 1\bar{1}0\rangle$, and $\{100\}\times\langle 011\rangle$ at different critical resolved shear stress ratios for the different slip systems. The prediction of the models is correlated with the results of x-ray diffraction measurements. Uniaxial deformation experiments on polycrystalline and single-crystal MgO samples were conducted *in situ* using white x-ray diffraction with a multielement detector and multianvil high-pressure apparatus at a pressure up to 6 GPa and a temperature of 500 °C. A deformation DIA was used to generate pressure and control at a constant deformation rate. Elastic strains and plastic strains were monitored using x-ray diffraction spectra and x-ray imaging techniques, respectively. The correlation of the data and models suggests that the plastic models need to be used to describe the stress–strain observations with the presence of plasticity, while the Reuss and Voigt models are appropriate for the elastic region of deformation, before the onset of plastic deformation. The similarity of elastic strains among different lattice planes suggests that the {*111*} slip system is the most significant slip system in MgO at high pressure and high temperature. © *2004 American Institute of Physics.*
[DOI: 10.1063/1.1738532]

I. INTRODUCTION

The relationship between the stress and strain fields in a polycrystalline system that is undergoing elastic or plastic deformation has been the focus of many materials science studies since the late 1920's.[1–3] Recently, it has become routine to measure the elastic differential strain field in both diamond anvil cells[4,5] and multianvil cells[6] using synchrotron x rays. In these experiments, the x rays pass through the sample along a path perpendicular to the compressive axis of a cylindrical stress field as illustrated in Fig. 1. The diffracted x rays sample the lattice spacings both parallel and perpendicular to the maximum stress. Detection can be by means of a two-dimensional system, such as an imaging plate or a charge coupled device (CCD) detector with monochromatic x rays, where the Debye rings are recorded as a function of the azimuthal angle, χ. Then, the lattice spacings parallel to the maximum stress axis at $\chi=0°$ can be compared with those parallel to minimum stress axis at $\chi=90°$. White x rays provide the same results with multiple solid-state detectors, used in conjunction with a conical slit in a multianvil press, located at $\chi=0°$ and $\chi=90°$.[6,7] These measurements have been possible with the use of x-ray transparent gaskets, usually Be for the diamond cell,[4] and x-ray transparent anvils, such as cubic boron nitride,[6] for the multianvil system.

Data obtained in this manner have been used to define the sample differential stress in the case that the single-crystal elastic moduli are known.[6] Fundamental to the interpretation of the relative strain parallel and perpendicular to the stress axis is the realization that the x-ray defined strain is an elastic strain. Processes, such as dislocation movement, atom diffusion, grain-boundary sliding, and recrystallization, will cause plastic strain, but will not alter the distance between lattice planes and, thus, will not be sampled by x-ray diffraction. On the other hand, stress will contribute to the distortion of the lattice via the equilibrium elasticity. Within the limitations of linear elasticity, the quantitative measure of stress is derived from the strain measurement following Hooke's law.[8,5]

The polycrystalline sample exhibits a complex stress–elastic strain field. The relationship between them is controlled by the elastic anisotropy in the elastic regime. In this case, stress can vary from point to point as the neighboring grains present varying boundary conditions to each grain.

[a]Electronic mail: lilli@notes.cc.sunysb.edu

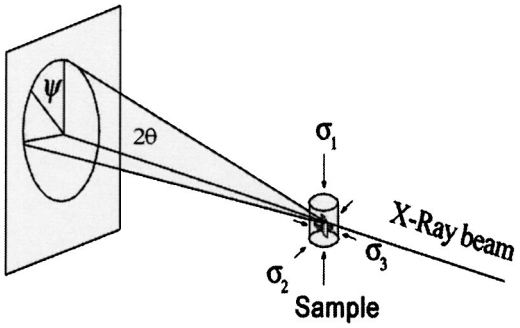

FIG. 1. Diffraction geometry for stress analysis. X rays travel perpendicular to the maximum compressive stress, σ_1, and are diffracted by an angle of 2θ. Lattice spacing is measured as a function of χ. d spacing is measured either by 2θ for monochromatic x rays or by energy at a fixed 2θ for white x rays. The $\chi=0°$ value corresponds to lattice planes whose normal are nearly parallel to the maximum stress direction while the $\chi=90°$ measurements yield lattice dimensions parallel to the $\sigma_2=\sigma_3$ directions.

Stress can also vary systematically with different subpopulations of grains that are defined by their orientation relative to the stress field. In this case, the elastically stiff axis will typically exhibit a larger stress and smaller strain than the elastically soft directions. Each diffraction line will give rise to a measure of the stress field in the sample, giving stress measures for distinct populations of grains, namely those whose orientations meet the necessary diffraction conditions. Singh[9] indicates the relationship between the strain field and the average stress field using the parameter, $\alpha=1$ to indicate a ''Reuss'' solid (uniform stress)[10,11] and $\alpha=0$ indicating a ''Voigt'' solid (uniform strain).[10] A value between 0 and 1 indicates a mixed boundary condition solid. The variation of stress and strain all fall within the broad bounds of the Reuss–Voigt limits. However, even the assumption of these bounds in the uniaxial compression will be challenged when plasticity plays a role. When the polycrystal is plastically deformed, several important changes occur. First, the x-ray diffraction is only sampling a portion of the total strain field. It does not reflect the plastic portion. Second, once the plastic deformation initiated, plastic properties may dominate the stress–strain state. In a single crystal, the Schmid factor, which represents the ratio of resolved shear stress on the slip plane versus the applied stress, becomes the dominating measure of anisotropy and the stress fields in the different grain populations now evolve to maintain the necessary stress on the dislocations to enable plastic deformation. In polycrystalline aggregates, five independent slip systems are required to accommodate the five independent strain components for plastic deformation.[12] This is the von Mises criterion. The minimum Taylor factor is used to identify the active combination in multiple slip systems in a similar fashion as the Schmid factor in single slip case. The Taylor–Sachs bounds (for details see Sec. III A) replace the Reuss–Voigt bounds. In general, the stress field of the various populations of grains will change radically. In a system with as high symmetry as face-centered cubic with 12 independent slip systems, the Taylor model predicts that the stress will vary by as much as 50% among the different grain populations.

In this article, we report data for polycrystalline MgO illustrating the effects of stress fields in a nonplastic, but stressed regime, and in a plastically deforming polycrystal at the same P, T conditions. The stress distribution among the different grain populations is drastically changed with plastic deformation. We also present a result of a self-consistent model for analyzing the stress relationships in a deforming solid.

This type of analysis will enable a more thorough understanding of deformation experiments conducted at high pressure. The average stress on the sample may simply be estimated by averaging the stresses defined for all of the subgrain populations. A more accurate estimate of the average stress will require forward modeling including specifying the slip systems and their constitutive relations.

This study illustrates that it is not reliable to measure single-crystal elastic properties in a material that is undergoing plastic deformation using the method suggested for high pressure studies.[4] That method requires that the Reuss bound be the correct bound for the solid. Thus, the variation of strain among the different populations indicates a variation in elastic properties since all grains are at the same stress. The observations reported here indicate that this assumption is badly violated once plastic deformation begins. Furthermore, once the solid has plastically deformed, the stress field may continue to reflect the effects of the Taylor-Sachs bounds.

II. ELASTICALLY DEFORMED POLYCRYSTALS

Stress is directly related to the elastic strain at any point within a polycrystalline aggregate by the well-known Hooke's law as in Eq. (1):

$$\sigma_i = c_{ij}\epsilon_j, \tag{1}$$

where repeated indices imply summation, σ_i and ϵ_j are the vector representations of stress and strain, while c_{ij} is the matrix form of the elastic stiffness tensor. If one could define the entire elastic strain field at any point in the sample, then the stresses can be specified through this relation. X-ray diffraction supplies some of the components of strain for subpopulations of the polycrystals, namely those that are in diffracting condition for the specific value of χ where an observation is made. Each diffraction peak is derived from a different subpopulation of grains. The strain represents the difference between the observed lattice spacing and that which would be produced by hydrostatic pressure. In a system with a uniaxial stress field, we define σ_1 as the maximum compressive stress and $\sigma_2=\sigma_3$ as the minimum compressive stress. We can then define a strain metric for a particular diffraction peak by $\gamma^{hkl}=(\epsilon_1-\epsilon_3)^{hkl}$. The strains, ϵ_1 and ϵ_3, measured at $\chi=0°$ and 90°, respectively, are also from different subpopulations of grains. If we assume that all of the grains of this subpopulation feel, on average, the same stress field, then γ^{hkl} becomes the differential strain for the grain subpopulation corresponding to the particular diffraction peak, (hkl). From this, we can define the subpopulation differential stress as in

$$\tau^{hkl}=(\sigma_1-\sigma_3)^{hkl}=E^{hkl}\gamma^{hkl}, \tag{2}$$

where E^{hkl} is Young's modulus corresponding to the (hkl) direction in the crystal. Young's moduli, as a function of (hkl) for different crystal symmetries, are given by Nye.[13]

In the last decade, these analysis techniques have been applied to determine single-crystal elasticity from polycrystalline x-ray diffraction[4,9,14] for MgO, iron, FeO, and other materials. The details of elastic moduli analysis have been described elsewhere.[9] In this approach, the differential stress is the difference between the two principle stresses in the radial and axial direction, while the hydrostatic pressure σ_P is the average of the three principle stress, as shown in

$$t=\sigma_1-\sigma_3,$$
$$\sigma_P=(2\sigma_1+\sigma_3)/3. \tag{3}$$

t differs from τ^{hkl} given above in that t represents the average differential stress and is independent of (hkl). The azimuthal angle χ is 0° when parallel to the unique stress axis and 90° when parallel to radial stress axis, as shown in Fig. 1. The d spacing is a function of χ, given by

$$d(hkl)=d_P(hkl)[1+(1-3\cos^2\chi)\gamma^{hkl}/3], \tag{4}$$

where $d(hkl)$ is the measured d spacing and $d_P(hkl)$ is the d spacing under the hydrostatic pressure σ_P. Equation (4) provides the basis for defining γ^{hkl} from measurements of d at least two values of χ. For cubic symmetry, γ^{hkl} is expressed as

$$\gamma(hkl)=3[m_0-3m_1\Gamma(hkl)],$$
$$\Gamma(hkl)=(h^2k^2+k^2l^2+l^2h^2)/(h^2+k^2+l^2)^2,$$
$$m_0=(t/3)[s_{11}-s_{12}], \tag{5}$$
$$m_1=(t/3)[s_{11}-s_{12}-s_{44}/2],$$

where s_{ij} are single-crystal elastic compliances, and m_0 and m_1 are combination elastic constants that reflect the (hkl) dependence. In fact, the variation of γ^{hkl} with (hkl) enables the determination of m_0 and m_1. Unless the stress, t, is known, then the most that one can determine about the elastic properties comes from the ratio of m_0 and m_1 that can yield the elastic anisotropy.

Assuming the stresses are uniform in the polycrystal (Reuss bound), the differential stress is given as

$$t=2G\langle\gamma(hkl)\rangle, \tag{6}$$

where G is the aggregate shear modulus at σ_P. A further constraint on the elastic moduli comes from knowledge of the isothermal bulk modulus K at σ_P through

$$1/(3K)=s_{11}+2s_{12}. \tag{7}$$

A combination of Eqs. (1)–(5) and the measurement of d spacings on different (hkl) will be enough to derive the three independent elastic constants for cubic crystal with known shear and isothermal bulk moduli. This analysis is based on an assumption of the Reuss bound for the elastic state of the material. Uncertainties result from the lack of knowledge of the actual elastic state of the aggregate.

The above analyses of the elastic properties relate the anisotropy in measured strain with anisotropy in elastic properties. If the anisotropy in strain is caused by properties other than elastic anisotropy, such as plasticity as discussed in the next section, then this method will fail. In particular, the experimental data obtained from the multianvil press demonstrate that the differential stresses for different diffraction vectors differ considerably from this assumption (see Sec. IV).

III. PLASTICALLY DEFORMING POLYCRYSTALS

Strain studies using Bragg scattering of conventional x rays[15] and neutrons[16] are well established. Due to the small penetration depth (several micron), early x-ray diffraction techniques were limited to the surface of the sample, and not able to represent the deformation and grain interaction inside the sample. On the other hand, the penetration depth of neutrons (on the order of cm) makes it possible to measure a bulk average of the elastic strains within subsets of grains. It has been recognized that residual stress and strain will be built up inside a plastically deformed material[17] and the overall result of the deformation process is a balance between elastic and plastic anisotropy.[18] Neutrons have been widely applied to study the residual stress in materials.[19–22] The elastic strains can be determined for different (hkl) reflections as described above. Different levels of lattice strain for different diffraction planes are a result of the anisotropic deformation process.

More recently, neutron studies have been conducted on samples undergoing tensile plastic deformation.[17,21] Using very similar diffraction geometries, elastic strains can be similarly observed varying with (hkl). Since they use standard deformation equipment, they are able to define the applied stress and macrostrain. Typical results are that elastic strains reflect elastic anisotropy at low stress, but can become highly nonlinear in the plastic region. For example, Ref. 20 reports the ratio of strain between the (*200*) and (*111*) peaks of stainless steel at 1.85 in the elastic region, and over 2.25 after 1% plastic strain. This increase reflects the failure of the weaker population of grains and thus increased stress on the stronger grains.

We assert that the Reuss–Voigt bounds limit the stresses and strains in the low stress elastic region with elastic anisotropy defining the strain anisotropy. In the plastic region, the stress–strain state is bounded by the Taylor–Sachs bounds, which reflect the plastic anisotropy arising from specific slip systems. In this latter region, the subpopulations of grains defined by (hkl) vary considerably. In the following sections, we discuss these models and the predictions of the stress fields. Once in this plastic region, the assumptions for defining elastic properties are no longer valid.

A. Plasticity models

In addition to the information from neutron experiments, extensive work has been done in modeling the aggregate deformation and studying the mechanisms of texture. Among those models, three are most common: Taylor–Hill model, Sachs model, and self-consistent models. The Taylor model[12] for calculating the uniaxial stress–strain relation for an aggregate requires five independent slip systems to accommodate the five independent strain components for plastic deformation, known as Von Mises Criteria. The plastic strain is homogeneous and independent of grain orientation in the Taylor model. Stresses are related to the geometry of the grains relative to the stress field and the slip systems. The

Sach model, which is also called the extreme lower bound, regards the aggregate as having the same stress for all grains. Again, the stress–strain field is governed by the geometry and strength of the active dislocation orientations.

The self-consistent model[23] is placed in between the upper-bound Taylor model and the lower-bound Sachs model. In the self-consistent model, both the elastic and plastic anisotropy can be incorporated into the plastic deformation process. This model is governed by the single-crystal slip mechanisms. The controlling parameters are the critical resolved stress and the hardening law.[17,24] The predicted strain and stress for different (hkl) lattice planes can be used to compare with the measured stress and strain for related (hkl) diffractions.

In the self-consistent model, the stress in each grain is found from the strain state, ϵ_c, and the instantaneous elastic–plastic grain stiffness, L_c, as $\sigma_c = L_c \epsilon_c$. The strain in a specific grain is related to the strain average of all grains by fourth-order concentration tensors A_c, as shown in

$$\begin{aligned} \sigma_c &= B_c \bar{\sigma}, \\ \epsilon_c &= A_c \bar{\epsilon}, \\ B_c &= L_c A_c (L)^{-1}, \end{aligned} \tag{8}$$

where σ_c is the resolved constituent stress, $\bar{\sigma}$ is the average stress for the aggregate, ϵ_c is the constituent strain, and $\bar{\epsilon}$ is the averaged strain for the aggregate. A_c is a function of L, L_c, and L^*, which are the overall stiffness, the grain stiffness and the constraint stiffness tensor, respectively, see Eq. (19) in Ref. 23. L_c is a function of the orientation (i.e., the three Euler angles), the elastic stiffness tensor, and the active slip systems. L^* is a function of the overall stiffness tensor and the Eshelby tensor, see Eq. (61) in Ref. 23.

Among these four variables, the constituent shear stress and strain are expressed in

$$\begin{aligned} \sigma_c &= L_c \epsilon_c = C_c (\epsilon_c - \epsilon_c^P), \\ \epsilon_c &= M_c \sigma_c = S_c \sigma_c + \epsilon_c^P, \end{aligned} \tag{9}$$

where M_c is the elastic–plastic compliance for the single crystals. C_c is the *elastic* stiffness and S_c is the compliance tensors. ϵ_c^p is the plastic part of the strain, which is the sum of weighted strain on active slip systems.

On the other hand, the critical resolved shear stress of the ith slip systems τ_i is related to the shear stress via[25]

$$\tau_i = \sum_i h^{ij} \gamma^j, \tag{10}$$

where γ^j is the shear stress of each slip systems. When the resolved shear stress on the ith slip system is larger than the critical resolved shear stress τ_i, the ith slip system is an active slip system and its action will contribute to the overall strain and stress of the aggregate; otherwise, it is an inactive slip system and is elastic. The critical resolved shear stress (CRSS) on each slip system is weighted by its own CRSS ratio. The CRSS ratio is controlled by the plastic anisotropy of the material and can be characterized by experiments on single crystal.

In the self-consistent model, the deformation of the polycrystalline aggregates is prescribed by the overall strain $\bar{\epsilon}$ along the compression direction, the stress and strain σ_c and ϵ_c can be calculated for all grains as well as the polycrystalline stress $\bar{\sigma}$. 2000 randomly oriented grains, defined by their Eulerian angles, are used to represent the inclusions in the aggregates. The stress and strain states for each individual grain are calculated independently then grouped according to their contribution to the elastic strain on (hkl) lattice planes. The elastic strain and stress on each (hkl) lattice plane, as well as the applied stress can thus be deduced. This model has its limitation in that the hardening laws are difficult to obtain for multiple slip in a single crystal, thus are empirical.

B. Predictions for MgO

Here, we adapted self-consistent models to predict stress and elastic strain states for MgO under uniaxial compression.[24,23] Three slip systems $\{110\}\langle 1\bar{1}0\rangle$, $\{111\}\langle 1\bar{1}0\rangle$, and $\{100\}\langle 1\bar{1}0\rangle$ are proposed as the possible active slip systems with different CRSS for each system.[14,26–29] At room temperature, the $\{110\}\langle 1\bar{1}0\rangle$ slip systems are reported to dominate,[14,26,29] while at a higher temperature slip on $\langle 111\rangle$ and $\langle 100\rangle$ may become active.[30–32]

We included these three slip systems in the self-consistent model with variable CRSS, which allows different yielding criteria for the initiation of plasticity on these systems. Stress and elastic strains for different (hkl) are then predicted for a uniaxial load with 1% total strain. Elastic constants for MgO (Ref. 33) are incorporated into the model. Results of these calculations are illustrated in Table I. The values of the CRSS, the calculated stress, and calculated elastic strain indicated in Table I represents the ratio of these quantities for the slip planes $\{111\}$, $\{100\}$, and $\{110\}$ and the diffraction vectors: (111), (200), and (220), respectively. The T absolute values of the stresses, as illustrated in Table I, are arbitrary. Thus, the ratios of stress and strain among different diffraction peaks are significant while their magnitudes depend on the assumed yield strength in the model. These calculations yield identical stresses whether the anisotropic elastic moduli are used or an isotropic modification are used, while the elastic strain changed considerably.

Seven combinations of CRSS are given here demonstrating the effects of each slip system or combination of them on the elastic strain and stress for each subpopulation of grains. This combination of CRSS values shows that (111) always has the highest stress among all the diffraction peaks. In fact, the stress for (111) is generally more than twice as high as the stress for (200) for all the possible combinations of slip systems. The elastic strain for diffraction peak (111) is also the highest among the three subpopulations, with the strain for peak (220) intermediate in value. On the basis of these models, we conclude that, in the plastic regime, the (111) diffraction peak is expected to have both the highest stress and the highest elastic strain for all combinations of slip systems that have been considered. This is in contrast to the elastic case, where (111) will exhibit the maximum stress and minimum strain. In addition, the stresses reflected in the different diffraction peaks vary by a factor of 2, far from being

TABLE I. Calculated differential elastic stress and strain for the diffraction peaks (*200*) and (*220*) relative to that for (*111*). Seven combinations of CRSS on the three slip systems are used. The CRSS values correspond to the relative strength of the three slip planes: {*111*}, {*100*}, and {*110*}. All systems share the ⟨*110*⟩ Burger's vector. The absolute values of the stress, which result from work hardening, are arbitrary. The stress and strain are calculated for a total strain of 1%, using the elastic properties of MgO (see Ref. 33) and for an isotropic modification of the MgO properties. In both cases, the calculated stresses are nearly identical. The elastic strains ratios are given here for both anisotropic and isotropic cases. In all cases represented here, the (*111*) diffraction peak exhibits the greatest elastic strain and the greatest differential stress.

Total strain	Relative CRSS			Relative stress			Relative elastic strain (Anisotropic)			Relative elastic strain (Isotropic)		
1%	{*111*}	{*100*}	{*110*}	(*111*)	(*200*)	(*220*)	(*111*)	(*200*)	(*220*)	(*111*)	(*200*)	(*220*)
1%	1	1	1	1	0.5	0.7	1	0.8	0.8	1	0.5	0.7
1%	1	1	10	1	0.6	0.8	1	0.9	0.8	1	0.6	0.8
1%	1	10	1	1	0.5	0.8	1	0.7	0.9	1	0.5	0.8
1%	1	10	10	1	0.5	0.8	1	0.8	0.9	1	0.5	0.8
1%	10	1	1	1	0.2	0.5	1	0.3	0.6	1	0.2	0.6
1%	10	1	10	1	0.6	0.6	1	0.9	0.7	1	0.6	0.7
1%	10	10	1	1	0.1	0.8	1	0.2	0.8	1	0.2	0.8

equal as is generally assumed for the Reuss state. In general, when {*111*} has a high CRSS ratio, the elastic strains for all diffraction peaks span a wide range. The {*111*} slip system needs to be an active slip system for the strains to be close to equal for the different diffraction peaks. As we see later, we observe that the strains for the diffraction peaks are quite close.

IV. EXPERIMENTAL OBSERVATIONS FOR MgO

The recent development of stress measurement techniques using synchrotron x-ray radiation provides the opportunity to measure the stress in a millimeter-sized sample of a polycrystalline material at high pressure and high temperature while it is being actively deformed. We have conducted uniaxial deformation experiments on both polycrystalline MgO and single-crystal samples oriented with (*111*) and (*100*) parallel to the maximum stress axis. The experiments were conducted using a large volume press with the deformation DIA (DDIA)[34,35] equipped with the 250 ton press (SAM 85) at the superconductor wiggler beam line (X-17B2) of the National Synchrotron Light Source. Details on SAM85 and the DDIA apparatus can be found elsewhere.[36,37]

Here, we report results from two experiments, Run Tan02 and Run MgO42. In the Tan02 run, two samples, a tantalum rod, and a presintered MgO powder, each 1.5 mm in length and 1 mm in diameter, were loaded into the cell assembly. In the MgO42 run, three samples, a thin layer of MgO powder, and two MgO single crystals, oriented along (*111*) and (*100*) respectively, each 1.5 mm in length and 1 mm in diameter, were used. Specimens were stacked on top of each other in the center of a BN sleeve, while separated from each other by a thin Ni foil or Au foil (about 20 μm thick). The BN sleeve was placed within a cylindrical graphite furnace, as shown in the cell assembly diagram (Fig. 2) for the DDIA apparatus. Opposed hard-alumina pistons were placed on both ends of the specimens to transmit the uniaxial stress from the driving anvils. These two pistons are separated from the specimens by thin metal foils. A mixture of amorphous boron and epoxy was used as pressure medium. A W3%Re–W25%Re thermocouple, situated next to the interface between the specimens, was used to measure the sample temperature. Temperature gradients within the specimens were less than 10 K/mm, as calibrated previously in similar cell assemblies. The data presented here are all for 500 °C. In the MgO42 run, the pressure was 5.7 GPa and the Ta02 experiment operated at two pressures: 2.3 and 4.5 GPa. The cell pressure precision was estimated within 0.5 GPa *in situ* using the MgO equation of state.

In these experiments, the pressure is increased to the first loading pressure, temperature is then increased to 500 °C, after which the deformation piston is activated providing a relatively constant strain rate between $10^{-6}\,s^{-1}$ and $10^{-5}\,s^{-1}$ for a period of 1 to 2 h. In the Tan02 experiment, the deformation was halted, temperature quenched, and pressure increased to the second point where the heating and deformation cycle was repeated. In the MgO42 experiment, further deformation was carried out at a higher temperature, but will not be discussed here as the differential stress decreased below the measurement threshold.

During both the Tan02 run and the MgO42 run, both specimen lengths were monitored by *in situ* x-ray radiography (describe in detail elsewhere),[38] using the thin metal foils, placed at the specimen ends which are opaque to the x-ray beam, as strain markers. Transmitted x rays were converted into visible light by the x-ray fluorescence of a YAG crystal placed downstream with respect to the cell assembly.

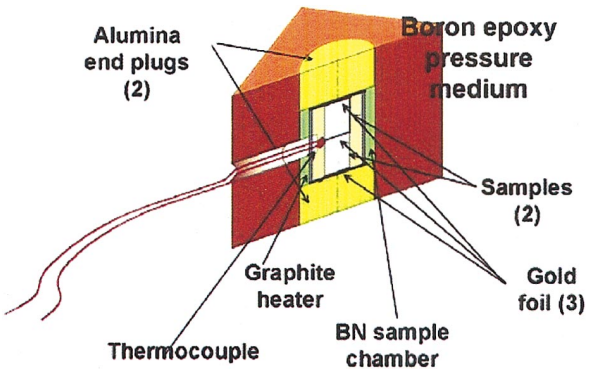

FIG. 2. (Color) A schematic diagram of the cell assembly used in the DDIA experiments. Hard alumina end plugs serve as pistons pushing on the stack of samples.

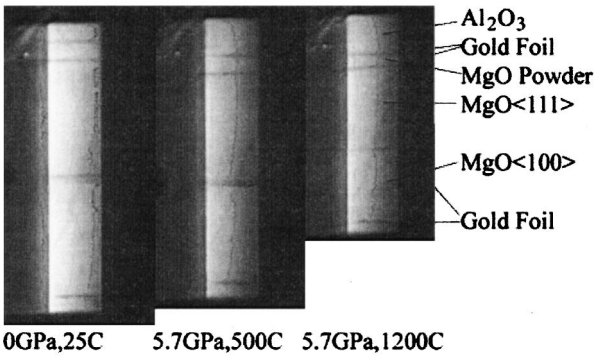

FIG. 3. Selected x-ray images for the ⟨*111*⟩ and ⟨*100*⟩ oriented single crystals of MgO in run MgO42. The metal foils separating the samples are dark lines in the image. The images are given for different pressure and temperature conditions.

The obtained images were magnified and then captured using a CCD camera. Typical x-ray images are shown in Fig. 3. The dark lines visible in each image of Fig. 3 are the metal foil markers at the top, or middle, and bottom of each specimen. Specimen time-resolved digital images were then processed using the method summarized elsewhere,[39] resulting in the high-pressure *in situ* measurements of specimen macroscopic strains and strain rates.

A. Plastically deformed MgO

The observations in the Tan02 run at both 2.3 GPa and 4.5 GPa are quite similar. The MgO sample length changes during the two deformation periods, illustrated in Fig. 4, yield strain rates of a few parts times $10^{-6}\,s^{-1}$ in the sample. Elastic strain, determined from two energy dispersive detectors located at $\chi=0°$ and 90°, yield γ^{hkl}, as defined above, for the (*111*) and (*200*) diffraction peaks. The (*220*) peak was not usable as it interfered with a fluorescence peak. Also illustrated in Fig. 4 are the elastic strains, γ^{hkl}, for these two peaks during the two deformation episodes. The elastic strain for (*111*) is slightly greater than for (*200*). Elastic strain is converted to stress using the relations defined above. Elastic moduli at the appropriate pressure and temperature are calculated as defined in

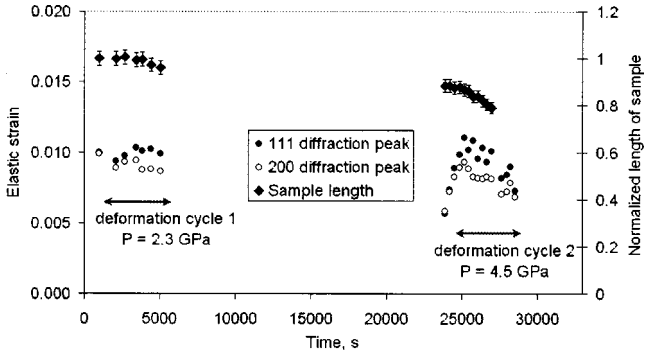

FIG. 4. Measured elastic strain from diffraction peaks (left-hand side scale) and sample length from images (right-hand side scale arbitrary units) for MgO in run Tan02 as a function of time. The two segments of data were collected a 2.3 GPa (left-hand side set) and 4.5 GPa (right-hand side set). Both sets were obtained during active deformation at 500 °C. The (*111*) diffraction peak consistently experiences the greatest elastic strain.

TABLE II. Elastic parameters for MgO.

	$P=0$ $T=300$ K	$\partial c_{ij}/\partial T$ (GPa/K)	$\partial c_{ij}/\partial P$
c_{11}	297.4	−0.062	8.6
c_{12}	95.57	0.011	1.3
c_{44}	156.2	−0.013	1.2

$$c_{ij}=c_{ij}(P=0,T=300\ \text{K})+P\,\partial c_{ij}/\partial P + (T-300)\,\partial c_{ij}/\partial T. \quad (11)$$

The elastic properties for MgO are given in Table II.[33] These data are substantially in agreement with those of others.[40,41]

The stress is illustrated in Fig. 5 for the two grain populations corresponding to (*111*) or (*200*) parallel to the maximum stress direction. The stress supported by the (*111*) population of grains is over 50% greater than the stress supported by the (*200*) population of grains. This stress–strain combination are outside of the Reuss–Voigt limits for an elastically stressed media. These bounds would require the stress on the (*111*) samples to be greater than that on (*200*) and the strain to be greatest for the (*200*) population. The combination of stress and strain, however, is quite compatible with the plastic self-consistent model discussed above.

In these uniaxial deformation experiments, elastic strain and stress were generated in the early stages of the deformation. Plastic flow should initiate once one of the slip systems reaches its yield point. The variations of the *d* spacing are still controlled by the elastic properties of and the stresses on the grains. However, the stress state of the aggregate is also affected by the plastic anisotropy and the total strain in the sample is the sum of the plastic and elastic strain. The strain, measured through the imaging technique, represents the total strain, which includes both the plastic and elastic strains. The strains, measured from x-ray diffraction spectra, represent only the elastic portion.

The actual stress state of the material, that is the average force per unit area acting on the polycrystal, will be some average of the stresses supported by the various populations of grains. Since the grains that are in a weak orientation will fail at a lower stress, they transfer some of the overall force to the stronger grains, which will then experience a stress

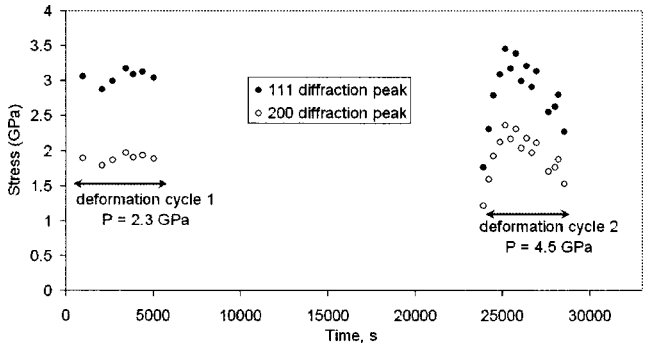

FIG. 5. Measured stress from diffraction peaks for MgO in run Tan02 as a function of time. The two segments of data were collected a 2.3 GPa (left-hand side set) and 4.5 GPa (right-hand side set). The stress inferred for the (*111*) diffraction subpopulation is significantly greater than that for the (*100*) population.

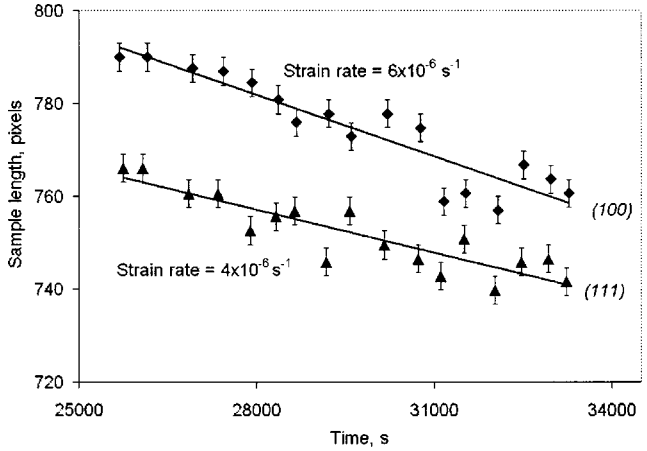

FIG. 6. Lengths of two single crystals of MgO as a function of time in run MgO42. The inferred strain rate for the (*111*) sample is about 50% less than that for the (*100*) single crystal.

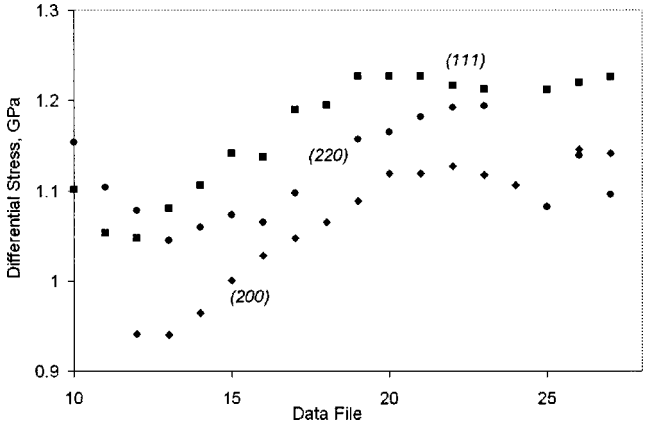

FIG. 8. Differential stress for the polycrystal with no observable plastic deformation in run MgO42. The (*200*) peak exhibits the lowest stress with (*111*) and (*220*) alternating with the highest stress. The data file id indicates the progression of measured diffraction spectra that span a period of about 8000 s during active deformation which was accommodated by the two single crystals that were in series with the polycrystal.

greater than the average. The strength of the deforming polycrystal will then be somewhere between the strength of the strongest population and that of the weakest population. The divergence of the stress reflects the plastic anisotropy of the solid with due respect of von Mises criterion in the polycrystal that need not apply to single-crystal strength.

B. Elastically deformed MgO

In the experiment MgO42, a thin polycrystalline MgO sample was placed in series with two single crystals along the high stress axis. Both single crystals exhibited considerable shortening while the polycrystal produced no measurable plastic deformation (see Fig. 6). The differential elastic strains in the polycrystal are illustrated in Fig. 7 for 500 °C and 5.7 GPa during active deformation. These elastic strains are about half of those measured in the MgO at similar conditions for the Tan02 experiment, suggesting that the differential stress was about one-half of that required for plastic deformation of the polycrystal, consistent with the lack of observed plastic flow in the MgO42 run. Apparently, the single crystals were significantly weaker than the polycrystal and buffered the stress.

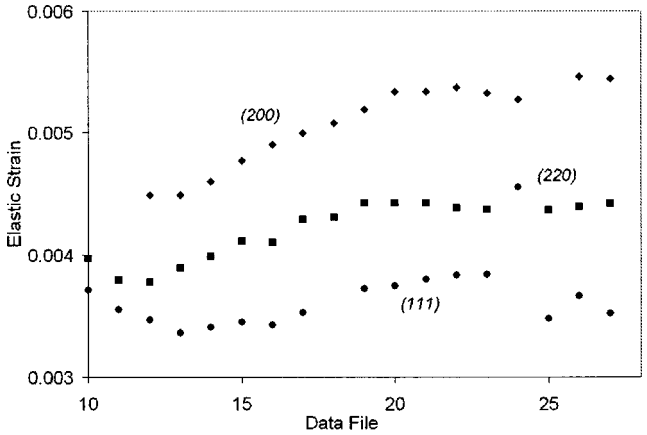

FIG. 7. Differential elastic strains for the polycrystal with no observable plastic deformation in run MgO42. The (*200*) peak exhibits the greatest elastic strain with (*111*) demonstrating the least. The data file id indicates the progression of measured diffraction spectra that span a period of about 8000 s during active deformation which was accommodated by the two single crystals that were in series with the polycrystal.

This experiment provides the opportunity to observe the stress–strain behavior of a polycrystal in the elastic regime. The MgO polycrystal, which is elastically stressed, does demonstrate the stress–strain field implied by the Reuss–Voigt bounds. The (*111*) strains in Fig. 7 are less than the (*200*) strain, and the (*111*) stress, in Fig. 8 are greater than the (*200*) stress. This state is consistent with a compromise between the uniform stress (the Reuss state) and uniform strain (the Voigt state), but closer to the Reuss state.

The deformation on the two single crystals allows us to estimate the relative strengths of the two orientations. The strength of these two crystals is compared through the respective strain rates of the two crystals that are placed in a serial manner inside a sample chamber that is forced to shorten with a constant rate. We observed that the crystal with (*100*) oriented parallel to the maximum compressive stress deformed about 50% faster than the crystal oriented with (*111*) in this direction, as shown in Fig. 6. Thus, the (*111*) orientation appears to be stronger than the (*100*) sample, but by only a relatively small amount.

V. DISCUSSION

Synchrotron x-ray sources, coupled with x-ray transparent anvils and gaskets, enable both multianvil and diamond anvil cells to be used in studies that determine the magnitude of the differential stress field at high pressure and temperature. With this powerful capability, we examine here some important considerations that are essential in interpreting the results. A mix of models and experimental results demonstrate the transition of controlling factors of the stress–strain state as the differential stress increases on the sample. Prior to plastic deformation, elastic anisotropy dominates the observations as mitigated by the Reuss–Voigt bounds. Once plastic flow proceeds, the stress–strain state is controlled by the agents of deformation through the orientation and

strengths the dislocations. These two states are often quite different, and assumptions based on one state will be seriously violated in the other state.

The MgO experiments demonstrate the different regimes. In an experiment where the polycrystal stress remained subplastic, as the sample was protected by the weaker single crystals, the stress–strain state is between the Reuss–Voigt bounds. In this case, the elastic strain for the (*111*) subpopulation was less than that for the (*100*) subpopulation, while the stresses were greater. Indeed, the relationships of the stresses and elastic strains appear as a compromise between uniform stress and uniform strain. Under the same pressure and temperature conditions, the situation changes when plastic deformation is in progress. Then, the elastic strain in the (*111*) subpopulation is greater than for the (*100*) group and the stresses are 50% higher. The elastic model cannot explain these results. However, the plastic model reproduces these results quite well. In these models, the stress and the elastic strain are predicted to be the greatest for the (*111*) subpopulation regardless of the dislocation system.

The self-consistent plastic model used here predicts that the elastic strains for the different subpopulations differ by a factor of 2 or more if the {*110*} slip planes are the primary slip system for MgO. We observe only a 10%–20% larger elastic strain for the (*111*) subpopulation. The self-consistent model takes into account the orientations of the dislocations and the stress field. It does not take into account the reduction of the stress field on the hard grains due to being surrounded by weak orientations. This effect may reduce the divergence of elastic strain among the grain populations. On the other hand, activation of the {*111*} slip planes makes the model much more consistent with the observations.

The relative strengths of the two single crystals support the possibility that the {*111*} slip plane is active in our experiments. If only {*110*} is active, then a crystal oriented with (*111*) parallel to the unique stress has a Schmidt factor of 0 on all slip planes and other mechanisms are needed to induce plastic flow. Low pressure low-temperature experiments[29] demonstrate a factor of 10 difference in strength for these two orientations. We observe that they are nearly equal, with the (*111*) orientation deforming about 50% faster than the (*100*) crystal. This would be consistent with flow that utilizes the {*111*} dislocations. Furthermore, previous results suggest that the {*111*} slip planes may become active at elevated temperatures.[30–32] We thus, tentatively conclude that the active dislocations were on the {*111*} slip planes in these experiments.

A polycrystal under stress distributes the stress and strain among the constituent grains. For a uniaxial stress, different subpopulations of grains will experience different elastic strains, plastic strains, and average stresses. The stress–strain state of different populations can be sampled with x-ray diffraction in that each diffraction peak represents an oriented subpopulation of grains and the orientation of the diffraction vector relative to the stress field enables this sampling. If only elastic deformation has occurred in the sample, then the stress–strain state is governed by the Reuss–Voigt bounds and the anisotropy of the observed elastic strains among the diffraction peaks reflects the elastic anisotropy of the material. Such measurements provide a pathway to define the single-crystal elastic properties at high pressure. Many diamond anvil experiments have pursued this possibility to measure these important properties. However, if the sample is stressed enough that plastic processes ensue, the strain anisotropy reflects the plastic anisotropy of the sample. Even for symmetries as high as cubic with multiple slip systems, the stress–elastic strain state generally violates the Reuss–Voigt bound. Inferences of the anisotropy of the diffraction peak strains in terms of elastic anisotropy are incorrect. The tools for measuring *in situ* stress remain an exciting frontier. Studies of rheology and elasticity will benefit from their exploitation.

ACKNOWLEDGMENTS

Funding was provided by the National Science Foundation through Grant Nos. EAR0135551 and EAR0229260, an REU program EAR 0139436 and by the support to beamline X17B2 through COMPRES (EAR 0135554). The authors utilized the facilities at the National Synchrotron Light Source of Brookhaven National Laboratory. This is MPI publication 320. One of the authors (W. B. D.) performed work under the auspices of the U.S. Department of Energy by the Lawrence Livermore National Laboratory under Contract No. W-7405-ENG-48. The authors thank Pam Burnley for her inspiring discussions and guidance. They also thank Dr. B. Clausen, of Los Alamos National Laboratory, for access to source codes of his self-consistent deformation model and for valuable insights regarding the self-consistent models.

[1] E. Kroener, Acta Metall. **9**, 155 (1961).
[2] P. R. Dawson, A. J. Beaudoin, and K. K. Mathur, in *Proceedings of the 15th Riso Int. Symp. on Mat. Sci.*, edited by S. I. E. A. Andersen (1994), Vol. 33.
[3] A. Molinari, G. R. Canova, and S. Ahzi, Acta Metall. **35**, 2983 (1987).
[4] H.-K. Mao, J. Shu, G. Shen, R. J. Hemley, B. Li, and A. K. Singh, Nature (London) **396**, 741 (1998).
[5] A. K. Singh, C. Balasingh, H.-K. Mao, R. Hemley, and J. Shu, J. Appl. Phys. **83**, 7567 (1998).
[6] L. Li, D. Weidner, P. Raterron, J. Chen, and M. Vaughan, Phys. Earth Planet. Inter. (to be published).
[7] J. Chen, L. Li, D. Weidner, and M. Vaughan, Phys. Earth Planet. Inter. (to be published).
[8] D. J. Weidner, Rev. Mineral. Ultrahigh-press. Mineral. **37**, 493 (1998).
[9] A. K. Singh, J. Appl. Phys. **73**, 4278 (1993).
[10] W. Voigt, *Lehrbuch der Kristallphysik* (Teubner, Berlin, 1928).
[11] A. Reuss, Z. Angew. Math. Mech. **9**, 49 (1929).
[12] G. I. Taylor, J. Inst. Met. **62**, 307 (1938).
[13] J. F. Nye, *Physical Properties of Crystals* (Oxford University Press, Ely House, London, 1957).
[14] S. Merkel, H. R. Wenk, J. Shu, G. Shen, P. Gillet, H.-K. Mao, and R. J. Hemley, J. Geophys. Res. **107**, 2271 (2002).
[15] I. C. Noyan and J. B. Cohen, *Residual Stress—Measurement by Diffraction and Interpretation* (Springer, New York, 1987).
[16] S. R. MacEwen, J. Faber, and A. P. L. Turner, Acta Metall. **31**, 657 (1983).
[17] B. Clausen, Thesis, Riso National Laboratory, 1997.
[18] T. Lorentzen, T. Faurholdt, B. Clausen, and J. Danckert, J. Strain Anal. **33**, 243 (1998).
[19] M. R. Daymond, M. A. M. Bourke, R. B. Von Dreele, B. Clausen, and T. Lorentzen, J. Appl. Phys. **82**, 1554 (1997).
[20] B. Clausen, T. Lorentzen, M. A. M. Bourke, and M. R. Daymond, Mater. Sci. Eng., A **258**, 17 (1999).
[21] M. R. Daymond and N. W. Bonner, Mater. Sci. Eng., A **340**, 272 (2003).

[22] M. R. Daymond, M. A. M. Bourke, and R. B. Von Dreele, J. Appl. Phys. **85**, 739 (1999).
[23] J. W. Hutchinson, Proc. R. Soc. London, Ser. A **319**, 247 (1970).
[24] B. Clausen and T. Lorentzen, *A Self-Consistent Model for Polycrystal Deformation, Description and Implementation*, Riso National Laboratory Report, Roskilde, Denmark, 1997
[25] R. Hill, J. Mech. Phys. Solids **14**, 95 (1966).
[26] M. S. Paterson and C. W. Weaver, J. Am. Ceram. Soc. **53**, 463 (1970).
[27] C. Meade and R. Jeanloz, J. Geophys. Res. **93**, 3261 (1988).
[28] S. M. Copley and J. A. Pask, J. Am. Ceram. Soc. **48**, 636 (1965).
[29] S. M. Copley and J. A. Pask, J. Am. Ceram. Soc. **48**, 139 (1965).
[30] I. Stretton, F. Heidelbach, S. Mackwell, and F. Langenhorst, Earth Planet. Sci. Lett. **194**, 229 (2001).
[31] D. Yamazaki and S.-I. Karato, Phys. Earth Planet. Inter. **131**, 251 (2002).
[32] R. Wenk, in *Plastic deformation of Minerals and Rocks*; edited by S. Karato and R. Wenk (Mineralogical Society of America, Washington, D.C., 2002), Vol. 51, pp. 291–329.
[33] H. Spetzler, J. Geophys. Res. **75**, 2073 (1970).
[34] W. Durham, D. Weidner, S. Karato, and Y. Wang, in *Plastic Deformation of Minerals and Rocks*; edited by S. Karato and R. Wenk (Mineralogical Society of America, Washington, D.C., 2002), Vol. 51, pp. 291–329.
[35] Y. Wang, W. B. Durham, I. C. Getting, and D. J. Weidner, Rev. Sci. Instrum. **74**, 3002 (2003).
[36] D. J. Weidner, M. T. Vaughan, J. Ko, Y. Wang, X. Liu, A. Yeganeh-Haeri, R. E. Pacalo, and Y. Zhao, in *High-Pressure Research: Application to Earth and Planetary Sciences*, edited by Y. Syono and M. H. Manghnani (Terra Scientific Publishing Company and American Geophysical Union, Tokyo and Washington, D.C., 1992), Vol. Geophysical Monograph 67, p. 13.
[37] M. T. Vaughan, D. J. Weidner, Y. B. Wang, J. H. Chen, C. C. Koleda, and I. C. Getting, Rev. High Pressure Sci. Technol. **7**, 1520 (1998).
[38] M. Vaughan, J. Chen, L. Li, D. Weidner, and B. Li, *Use of X-ray Imaging Techniques at High-Pressure and Temperature for Strain Measurements* (Universities Press, Hyderabad, India, 2000), pp. 1097–1098.
[39] L. Li, P. Raterron, D. J. Weidner, and J. Chen, Phys. Earth Planet. Inter. **138**, 113 (2003).
[40] C.-S. Zha, H.-K. Mao, and R. J. Hemley, Proc. Natl. Acad. Sci. U.S.A. **97**, 13494 (2000).
[41] S. V. Sinogeikin and J. D. Bass, Phys. Rev. B **59**, R14141 (1999).